NREL/TP-411-8116 • UC Category: 1262 • DE95009272

Experimental Study of the Factors Governing the Staebler-Wronski Photodegradation Effect in a-Si:H Solar Cells

Annual Subcontract Report
1 March 1994 – 31 March 1995

D. X. Han, L. E. McNeil, K. D. Wang, C. N. Yeh
University of North Carolina
Chapel Hill, North Carolina

NREL technical monitor: W. Luft

National Renewable Energy Laboratory
1617 Cole Boulevard
Golden, Colorado 80401-3393
A national laboratory of the U.S. Department of Energy
Managed by Midwest Research Institute
for the U.S. Department of Energy
under contract No. DE-AC36-83CH10093

Prepared under Subcontract No. XAN-4-13318-09

August 1995

NOTICE

Available to DOE and DOE contractors from:
Office of Scientific and Technical Information (OSTI)
P.O. Box 62
Oak Ridge, TN 37831
Prices available by calling (615) 576-8401

Available to the public from:
National Technical Information Service (NTIS)
U.S. Department of Commerce
5285 Port Royal Road
Springfield, VA 22161
(703) 487-4650

Printed on paper containing at least 50% wastepaper and 10% postconsumer waste

PREFACE

This report covers the first year study to understand the mechanisms of the Staebler-Wronski photodegradation in a-Si:H solar cells for the purpose of proposing methods to minimize the effect under subcontract No. XAN-4-13318-09 during the time period of March 1, 1994 - March 31, 1995.

The work at Chapel Hill was performed by:
D. X. Han - P.I.
L. E. McNeil - co-P.I.
K. D. Wang - Research Associate
C. N. Yeh - Ph. D student

The samples obtained through collaboration with L. Y. Yang, Y. M. Li at Solarex, X. M. Deng at Energy Conversion Devices (ECD), S. Hegedus at Institute for Energy Conversion (IEC) at Delaware, R. Crandall and H. Mahan at National Renewable Energy Laboratory (NREL), and R. Vanderhaghen in Laboratoire de Physique des Interfaces et des Couches Minces (LPICM), UPR 258-CNRS, Ecole Polytechnique, Palaiseau, France. We have also benefited from numerous discussions with our Condensed Matter colleagues: Y. Wu, J. P. Lu. At other institutions we have collaborated with R. Vanderhahgen in France, G. J. Adriaessens at K. University Leuven, Belgium, L.Y Yang at Solarex, and mostly with H. Branz, R. Crandall, and B. Vonroed at NREL.

SUMMARY

During the contract year, March 1, 1994 - March 30, 1995, we have continued our experiments on Electroluminescence (EL) and transient forward bias current (TFC) as well as photocurrent before and after light soaking. We continued our EL spectrum analysis on p-i-n device with and without SiC:H buffer in p-i interface. We have started a program to study the SWE in p-i-n solar cells made with and without H_2-dilution which is collaborated with Solarex. In collaboration with L. E. McNeil we study the carrier recombination in p-i-n cells by both photoluminescence (PL) and EL. In collaboration with R. Vanderhahgen in France, we study photogain in a-Si:H p-i-n and n-i-p devices. In collaboration with G. J. Adriaessens at K. University Leuven, Belgium we study TFC in p-i-n devices. In collaboration with Y. Wu we study the local Si-H bonding configuration in hot-wire samples by nuclear magnetic resonance (NMR).

We have concentrated on determining the factors controlling SWE, on determining the correlation of EL data to the cell structure or preparation conditions, such as the effect of buffering and of H_2-dilution, by EL measurements. The results of EL will be given in section I.

In section II we present our results of $\mu\tau$-product from photocurrent gain as a function of junction properties, and i-layer properties.

In section III we report the progress of electronic profiling studies in p-i-n structures.

Section IV shows the results of TFC . TFC as a function of applied voltage for different junction before and after light-soaking will be given.

Section V gives modeling work to explain both our EL and TFC results.

Section VI gives the preliminary results on new materials studies by NMR.

Perhaps the most interesting and important results were obtained on the EL efficiency and EL spectra in solar cell devices. We found that the room temperature EL effective efficiency, EL/J_F is proportional to the initial energy conversion efficiency regardless of preparation conditions. Furthermore, we found that the energy spectrum of EL defect band varies from cell to cell. The narrower the EL band the better the cell performance and the better stability.

Our research last year has results in seven papers (see publications) and the submission of four quarterly reports, one final subcontract report (91-94), one annual report, and one report for DOE PV program peer review (94.12).

Table of Contents

List of Figures

Introduction

One of the major factors limiting the solar cell performance is light-induced degradation, the so-called the Staebler-Wronski effect (SWE). To minimize this effect we must know where and how defects are formed. Many models have been proposed for the SWE, but to date none of these have been definitely proven. This is especially true in device structures, e.g. it is not clear how junction and interface properties are degraded. The mechanisms and kinetics of the SWE could clearly depend upon junction and i-layer properties, such as, buffering, and H_2-dilution. Our work is aimed at determining the source, position and precursor states involved in the SWE in solar cell structures.

The SWE clearly produces additional states deep in the gap. The questions are: are the important states located primarily near the junctions or are they located in the bulk of the i-layer? How do the metastable changes of deep states correlate to the photodegradation of the solar cells? It is clear that the quasi-Fermi level is increased toward the band edges under illumination or current injection, whether or not the SWE occurs related with non-relaxed states? One must understand whether unrelaxed defect states are important and what governs the energy and time scale of this relaxation. It is the purpose of our research to address all of these questions through studies of EL, electric field profiles, photo gain, and transient current properties and degradation in p-i-n samples. In addition, the NMR study is a new means for us to explore the Si-H local bonding configurations in new materials, such as hot-wire samples.

1) Electroluminescence (EL)
EL is a result of recombination in both the bulk and junction regions. By studying the total efficiency we can determine the recombination both in the bulk and in the interfaces; by studying the spectral distribution we can determine which states are important, while degradation of EL spectrum as a function of light-soaking time will reveal the kinetics.

2) Photocurrent Gain Under Forward Bias
The gain is obtained from the ratio of the forward-bias to reverse-bias photocurrent. Photo gain yield is the $\mu\tau$ product in a solar cell configuration. We have studied the gain as a function of degradation, junction properties and thickness to determine how the lifetime of the carrier depends upon these parameters.

3) Electronic Profiling

The electric field profile varies depending upon where recombination takes place. We have studied PL spectra and combined the results with the EL results to explore where and how the recombination takes place in a-Si:H solar cells.

4) Transient Forward Currents (TFC)
TFC can probe both shallow and deep traps. Transient double injection current is a tool to study the energy relaxation of excited defect states which may be involved in the kinetics of the SWE.

5) Modeling
Interpretation of experimental results is vital in order to formulate suggested improvements in solar cell performance. In most sections we present results with discussions. We will discuss a special issue in the modeling section.

6) NMR
Since Si-H bonds play an important role in the metastability, we have studied local Si-H bonding configurations by NMR to find why the new hot-wire material does show better stability.

Results

I. Electroluminescence (EL)

I.1 Introduction

The performance of a-Si:H solar cells is determined, to a large extent, by the density of gap states (DOS) in the intrinsic i-layer. Much understanding of the DOS and its function in electron transport has become available in recent years. Several techniques are available to characterize the DOS in a-Si:H films. However, the results and the interpretation of the results from the various techniques have often been in disagreement with one another. On the other hand, scientists in the PV industry have found that the electronic parameters in the films, such as mobility-lifetime product, $\mu\tau$, obtained from time-of-flight (TOF) measurements, DOS obtained from constant photocurrent method (CPM) measurements; as well as the structure parameters, such as the hydrogen bonding configuration and the microvoid concentration obtained from infrared absorption (IR) and small angle X-ray scattering (SAXS), do not correlate well with cell performance.[2] Therefore, a suitable technique to measure recombination in real solar cells is needed. EL spectroscopy measurements were carried out for this purpose. Our previous EL thickness-dependence and lifetime-distribution studies [3,4] have been shown to yield information on where recombination takes place, and what pathways for the recombination are important in p-i-n structures. Further results in solar cells were obtained during the last contract year.

Under forward bias, electrons and holes are injected into the i-layer from opposite sides of the diode. EL is the result of excess electron-hole recombination in the i-layer, including the interfaces. At low temperature, the tail-to-tail transition gives the main-band luminescence, EL_m. At room temperatures, the tail-to-defect radiative recombination gives the defect-band luminescence, EL_d. The generation rate of EL, g, is defined as the number of injected electrons that recombine with holes per cm^3, per second. This can be expressed in terms of the density of forward bias current, J_F, $g = J_F/eL_D$. The EL quantum efficiency, EL/g, then can be expressed as [5]

$$\eta_{EL} = \frac{EL}{J_F/eL_D} \qquad (1.1)$$

where e the charge of an electron, $L_D=\mu\tau E$ the drift-length, $E = V/L$ is the electric field across the i-layer, and L the thickness of the i-layer. Since for $\mu_n\tau_n >> \mu_p\tau_p$, the electron current dominates the forward current, one has $L_D\approx\mu_n\tau_n E$.

I.2 Samples and experimental conditions

A micro-refrigerator stage was used to hold the sample in the temperature range of 80 to 300 K. The applied voltage was obtained from a programmable pulse generator. A standard lock-in technique was used to collect the EL signal. The contribution of thermal radiation to the signal was less than 2% of the total signal. The EL spectra were recorded by a Ge detector. The response curve of the detector and the system optics was calibrated by using a linear response detector.

We study samples obtained from the other team members, Solarex, ECD, IEC, and NREL, and also from our collaborators in France. The sample preparation conditions and cell performance are listed in Table I. The substrate surface was textured to avoid interference fringes. The top contacts were Ag, Al or ZnO, and the area was 0.1 to 0.3 cm^2. The i-layer thicknesses were 0.2, 0.4, 0.5, and 0.55 mm. The cell structures were either p-i-n, n-i-p, or p-b-i-n. For NMR studies, the samples were prepared by NREL on Al foil substrates.

Table I Sample Preparation Conditions and Cell Performance

Sample I.D.	Structure	i-layer Deposition	H content (at.%)	V_{oc} (volt)	J_{sc} (mA/cm^2)	FF (unit)	Efficiency (%)
TH125	i-layer on Al foil		3				
i131	i-ayer on Al foil		8-10				
202	3 μm i-layer	H-dilution	8-10				
522		PECVD	8-10	0.952	17.0	0.560	9.0
533		PECVD	8-10	0.939	16.5	0.628	9.8
330		PECVD	8-10	0.860	13.0	0.690	7.9
25		PECVD	8-10	0.810	14.0	0.660	7.5
26	with buffer	PECVD	8-10	0.850	14.8	0.660	8.3
10		H-dilution	8-10	0.888	14.3	0.686	8.7
20		pure-silane	8-10	0.862	14..2	0.684	8.4
82		PhotoCVD	11	0.810	12.0	0.660	6.5
88		PhotoCVD	7	0.799	11.9	0.600	5.5-6
55	with buffer	PhotoCVD	7	0.843	14.0	0.680	8-8.3

I.3 EL Results

Effective EL efficiency as a function of solar energy conversion efficiency

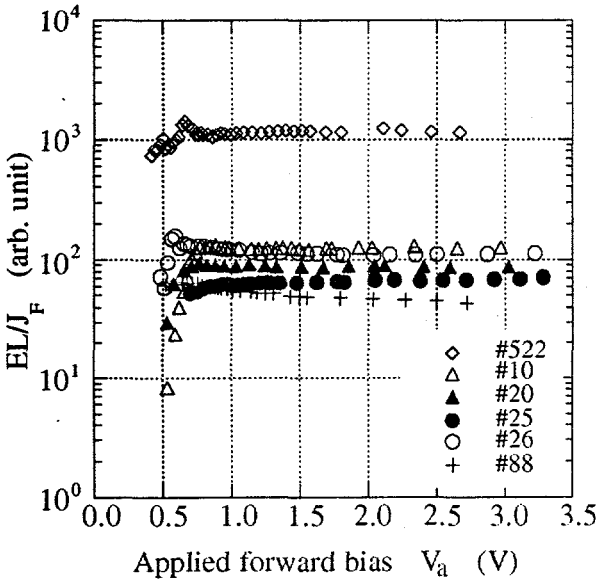

Fig. 1 EL/J_F vs. forward bias for samples #522, #10, #20, #25, #26, and #88 at 300 K.

According to Eq. (1.1) the EL efficiency is $\eta \equiv \frac{I_{EL}(e\mu_n\tau_n E)}{J_F}$ where the value of $\mu_n\tau_n \approx 10^{-5}$ cm^2/V for all the cells in the initial state. As shown in Fig. 1, the electric field across the i-layer in a certain range has no effect on the efficiency, so that EL/J_F is the effective efficiency of EL. Fig. 1 plots EL/J_F curves as a function of applied voltage at 300 K for six samples made by PECVD and PhotoCVD in different laboratories. The sample IDs are listed in the figure and the corresponding solar cell parameters are listed in Table I. One can see that the EL signal was measurable from about 0.5 V forward bias regardless of the device structures and their preparation conditions. The EL efficiencies increase with applied voltage in the low injection region when the external field is smaller than the built-in field. As the applied forward voltages increase, there is a transition region between 0.7 V to 1.0 V. We found that the EL effective efficiency in the applied voltage range

of 0.8 V to 3 V is almost constant. Therefore, one can use room-temperature EL/J_F with $V_a >$ 0.8 V as a characteristic parameter for p-i-n or n-i-p cells. This parameter is a synthesis of the radiative recombination that is inversely proportional to the defect density in both the i-layer and the interfaces; and it will be enhanced by multiple reflections by using a reflection substrate.[6]

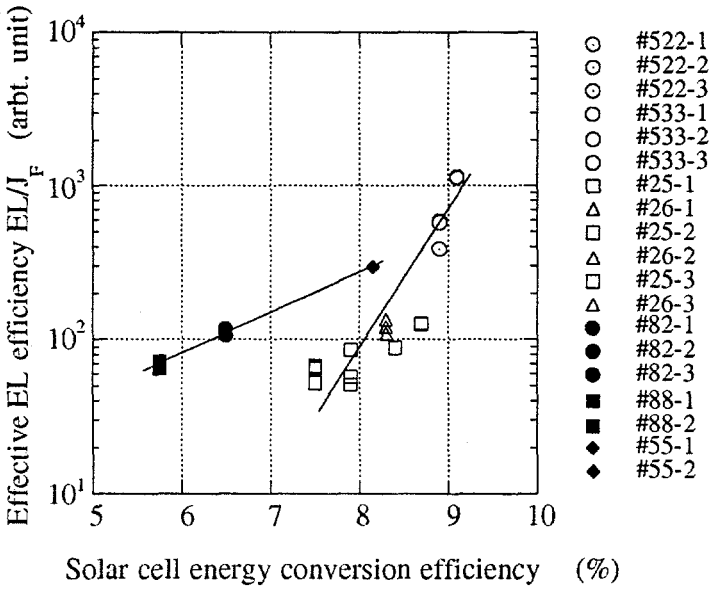

Fig. 2 EL efficiency vs. solar cell conversion efficiency for the cells listed in Table I. Several dots were measured for each sample with the same I.D.

Figure 2 plots the EL effective efficiency as a function of the solar cell conversion efficiency for twenty dots made at different laboratories as listed in Table I. One can see that the data from cells made by PECVD follow the same line. The data from the cells made by PhotoCVD follow another line. Notice that these cells are all in the initial state. We found that the room temperature EL effective efficiency, EL/J_F is proportional to the solar cell energy conversion efficiency regardless of preparation conditions. Light-soaking increases the defect density and decreases the $\mu_n\tau_n$ product. Therefore, the effective efficiency EL/J_F is no longer a good parameter for the measure of the defect density, one must use $\eta \equiv \frac{I_{EL}(e\mu_n\tau_n VL)}{J_F}$ to describe the EL efficiency.

EL spectra of samples with different preparation conditions

The EL spectrum of a-Si:H is typically characterized by two bands: the 1.2 eV main band (EL_m) is due to tail-to-tail radiative recombination, and the 0.9 eV defect band (EL_d) is due to defect-to-tail radiative recombination. The line shape of the main band depends on the width of the band tail states [9] while the line shape of the low-energy band may depend on the distribution of the deep traps. We have measured the EL spectra for the samples listed in Table I and found there is a correlation between the line shape and the cell performance. Fig. 3a shows the EL line shape at 80 K for samples #522, #10 and #20, which have a similar density of defects, DOS $\leq 10^{16}$ cm^{-3}. One can see that besides the 1.2 eV EL_m dominant peak there is a low-energy shoulder which indicates that there are more deep traps in cell #20 (made without H_2-dilution), but many fewer in #522. We further show, in Fig. 3b, the EL spectra for the same group of samples at 300 K. Comparing the spectrum line shape with the cell's parameters listed in Table I, one finds the energy conversion efficiency is 8.4, 8.7 and 9.0 for cells #20, #10 and #522, respectively. It is clearly that the narrower the EL band, the better the cell performance.

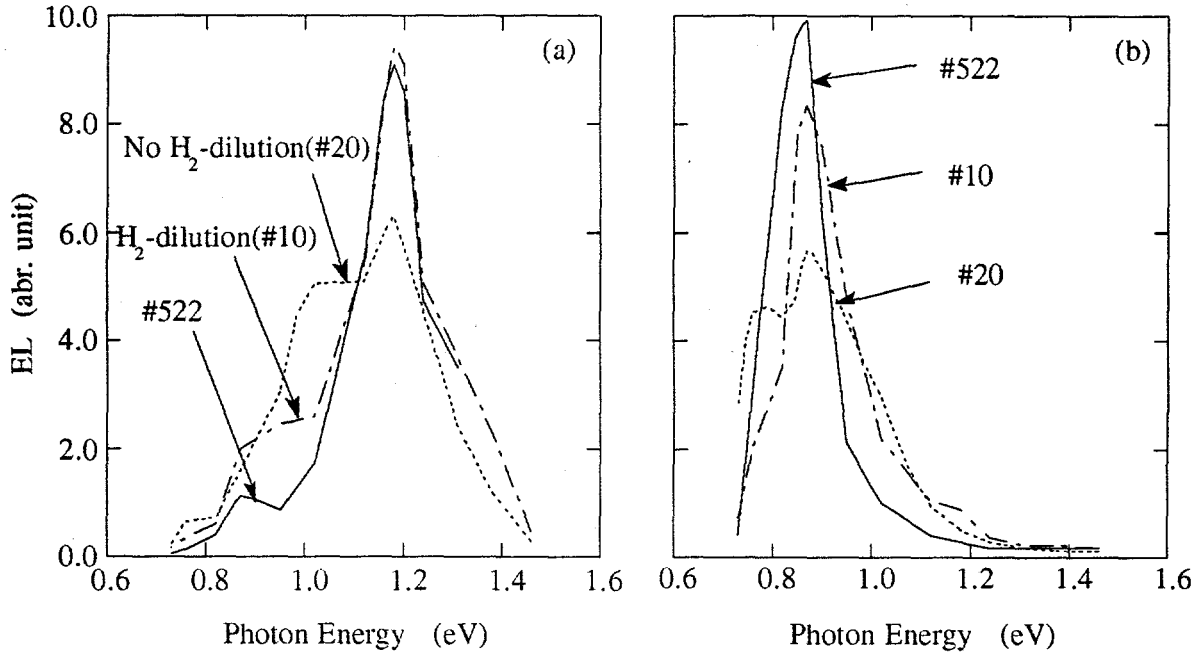

Fig. 3. EL spectra for cell #522, and cells #10 and #20 made with and without H_2-dilution.
(a) under 4 V forward bias at 80 K , and
(b) under 0.8 V forward bias at 300 K.

Quasi-Fermi level Splitting and Open-circuit voltages, V_{oc}

As we discussed above that there is a correlation between the EL line shape and the cell performance. A thin graded SiC:H composition buffer layer (b-layer) at the interface between the wide bandgap a-SiC:H p-layer and the a-Si:H i-layer improves the cell properties by increasing the V_{oc} and the overall device performance. We compared the EL spectrum line-shape in a pair of samples, #26/#25, made by PECVD and found that the p-b-i-n cell #26 shows stronger main-band luminescence than the p-i-n cell #25. The other cell made by PhotoCVD with a buffer layer, #55, showed even stronger enhancement of the main-band luminescence than the cell without a buffer layer, #88. Interestingly, a similar spectrum can be obtained in the p-i-n cell by increasing the applied voltage. With increasing V_a, current injection increases which shifts the quasi-Fermi level as much as $\Delta E_{qf} = kT\ln(J_{F2}/J_{F1})$.[7] We obtained $\Delta E_{qf} \approx$ 40-50 meV in the p-i-n cell to match the ΔEL between p-b-i-n and p-i-n cells as shown in Fig. 4a and 4b. The required increase of applied voltage is just enough to shift the quasi-Fermi level an amount equal to the increase of the V_{oc} as seen in Table I. A higher current density also means a higher occupation of the tail states that results in a stronger high-energy luminescence, EL_m. Figures 4a and 4b show the comparison of the EL spectrum modification by either a buffer layer or an increase of the applied voltage at 300 K and 200 K, respectively. On the other hand, the function of the buffer layer is to reduce deep states around the p-i interface, [8] and therefore the occupation of tail states, and then the main-band EL_m is enhanced in the diode with buffer layer. In photovoltaic mode the buffer drives the electrons away from the p-i interface, and leads to less recombination which increases V_{oc}. The question is whether there are any changes in the i-layer. Since the luminescence signal is mainly from the i-layer, based on the EL spectra shown in Fig. 4 the carrier occupation in the i-layer must be changed by inserting a buffer layer. This can be due to the decrease of midgap recombination near the p-i interface. However, a decrease of the deep

states in the i-layer is not excluded, if the better lattice match between the a-SiC:H p-layer and the a-Si:H i-layer releases the strain in the i-layer.

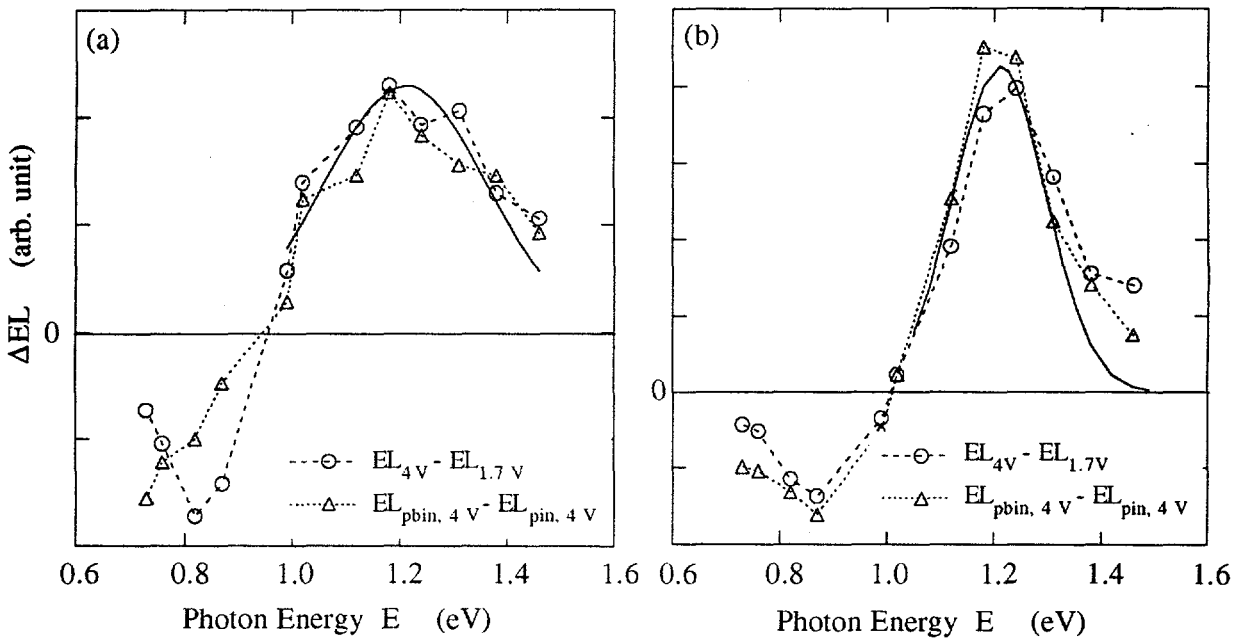

Fig. 4 Modification of EL spectra with a buffer layer or with an increase of applied voltage in #26 p-b-i-n and #25 p-i-n cells. The solid lines are a guide for the eye. (a) at 300 K, (b) at 200 K.

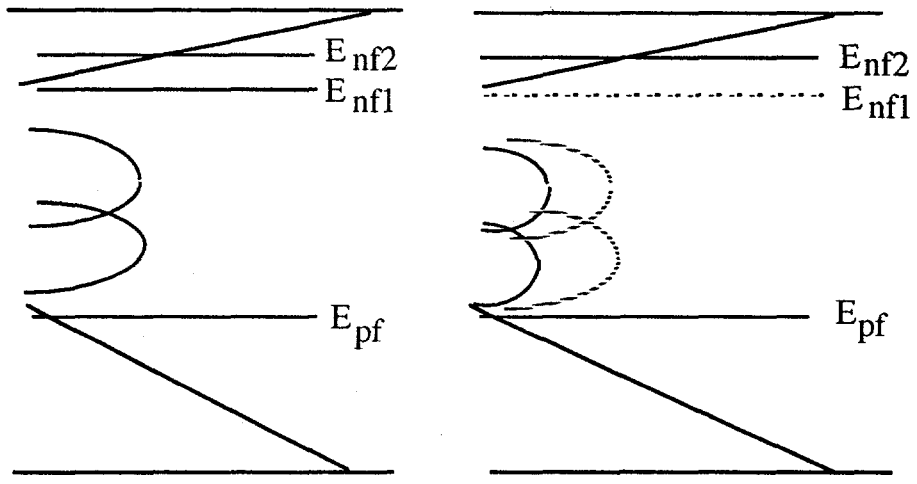

(a) (b)

Fig. 5. Schematic diagram of the position of the quasi-Fermi level
(a) in a p-i-n cell under 1.7 V and 4.0 V forward bias, respectively,
(b) in a cell under 1.7 V with p-i-n and p-b-i-n structures. The dotted lines describe the DOS and E_{fn} in the p-i-n structure, the solid lines are the corresponding values in the p-b-i-n structure.

We use a schematic diagram to describe the function of increasing the applied voltage and of inserting a buffer-layer. We found that #25 p-i-n and #26 p-b-i-n cells show identical J_F-V and

J_F-T curves when $V \geq 0.9$ V ($J_F \geq 10$ mA/cm^2). Therefore, we assume that the same voltage occurs across the i-layer under the same forward bias. In Figure 5 the shift of the quasi-Fermi level position indicates the changes in the carrier occupation. This diagram indicates that the V_{oc} is simply related to the quasi-Fermi level splitting obtainable under forward bias and that the buffer layer serves to increase this splitting.

Light-soaking effects on EL efficiency

We next show light-soaking effects on EL efficiency and the importance of the correct definition of the generation rate of EL for the interpretation of the light-soaking effects. The #10 cell was exposed to 2000 W/m^2 light for a series of equal-time light-soaking steps. Fig. 6 plots I_{EL}/J_F vs. J_F. Surprisingly, the EL efficiency, I_{EL}/J_F, appears to increase with light-soaking. After 30 hr., the maximum I_{EL}/J_F is about a factor of 2 larger than in State A. If the non-radiative recombination had been enhanced by light-soaking we would not expect the radiative recombination efficiency to increase. According to Eq. (1.1), we conclude that the $\mu_n\tau_n$ product is decreasing with light-soaking. When we use the correct expression for the generation rate and apply reasonable values of the $\mu_n\tau_n$ product, the results of the light-soaking effect on EL efficiency become more reasonable. Our results are replotted in Fig. 7 with $\mu_n\tau_n(A) \approx 10^{-5}$ cm^2/V in State A, and $\mu_n\tau_n(B) \approx 10^{-6}$ cm^2/V after 2 hr light-soaking. In Fig. 7 we see that the EL efficiency, $\mu_n\tau_n I_{EL}/J_F$, does decrease roughly an order of magnitude upon light- soaking.

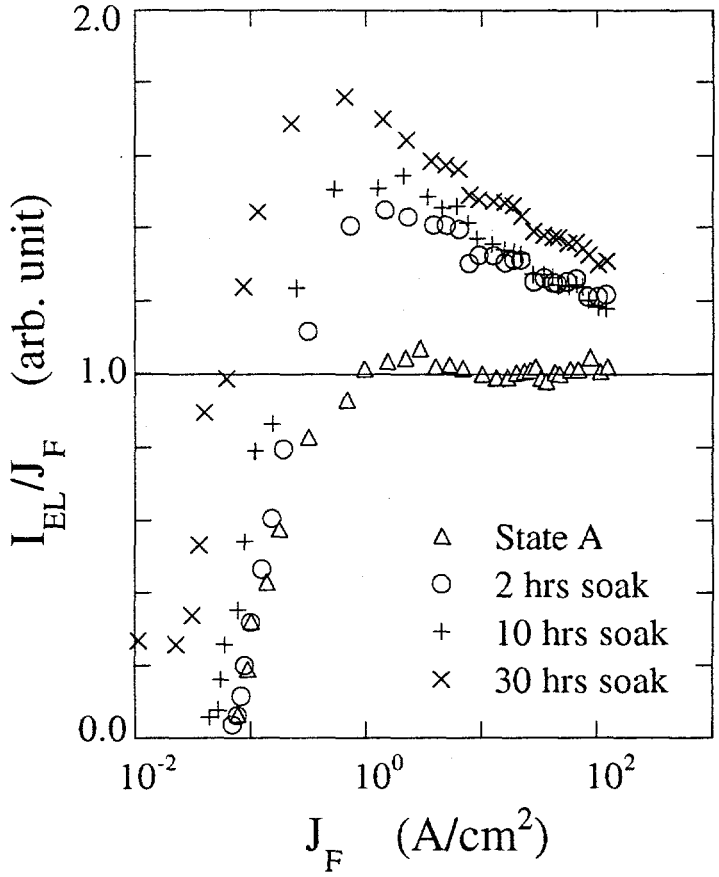

Fig. 6 Light-soaking effects on EL efficiency at room temperature. Legend shows light-soaking times for a 0.5 μm p-i-n device (#10).

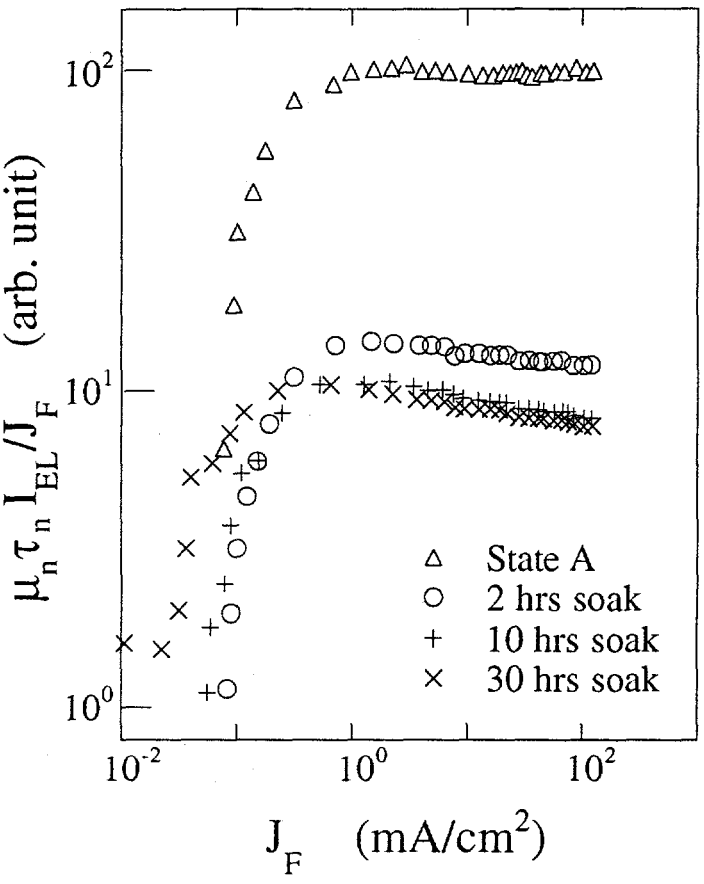

Fig. 7 Same data as in Fig. 6 multiplied by the $\mu_n\tau_n$ product of its exposure state.

I. 4 Conclusions

We have demonstrated that the results from EL measurements correlate well with the solar cell parameters. In summary, EL measurements appear to form a complement to the existing CPM and PDS techniques to characterize the quality of the intrinsic material (i-layer) and of the correlated p-i-n cells. The main conclusions that we draw from these EL studies are:

1) The EL effective efficiency at room temperature is proportional to the solar cell initial efficiency. Since the EL efficiency is inversely proportional to the defect density in both the i-layer and the interfaces, the interface contribution can be evaluated with the known bulk density of defects. Further study of to separate the contributions of interface and bulk recombination is needed.

2) We found that, at room temperature, the energy spectrum of EL defect band, EL_d, varies from cell to cell. The narrower the EL band, the better the cell performance, which indicates that **not only the total density of** defects but also **their energy distribution is** crucial for the cell performance.

3) EL spectra of the photodegradation effect give useful information about how those deep states are responsible for the degradation. EL spectra of the photodegradation effect in both H_2-diluted and non H_2-diluted solar cells are being undertaken.

4) The enhancement of the EL main-band is correlated with the presence of the SiC:H buffer-layer which is used to increase V_{oc}. The EL results can be explained by a decrease of the

density of deep states near the p-i interface, but a decrease of the deep states in the i-layer is not excluded.

5) The photodegradation effect on EL efficiency is dominated by the decrease of the $\mu\tau$ product. The effective EL efficiency EL/J_F should not be used to characterize a solar cell without taking the $\mu\tau$ product into account.

II. Photocurrent gain

For the photogain studies, we have worked in collaboration with Regis Vanderhaghen of LPICM, Ecole Polytechnique, France. A paper entitled "Interface effects on double injection current and photocurrent in a-Si:H n-i-p and p-i-n diodes", is to be published in J. Non-Cryst. Sol.(1995).

II.1 $\mu\tau$ product in p-i-n devices deduced from photogain

The $\mu\tau$ product is the most important transport parameter of the i-layer for a-Si:H solar cells. Photoconductive gain gives directly the $\mu\tau$ product in a device configuration. In the case of electron-hole double injection, the net charge density in the diode, eN_{sc}, is limited to roughly CV/L where C, V, and L are the capacitance of the sample, the applied voltage, and the i-layer thickness, respectively. When the carrier lifetime τ_n is greater than the transit time t_n, the injected carrier density N^- and N^+ can each be much greater than CV/eL . One can write the net space charge density eN_{sc} as follows:

$$eN_{sc} = CV/L = e(|N^+| - |N^-|)$$
$$\cong e[(p + p_t) - (n + n_t)], \qquad (2.1)$$

where n (p) and n_t (p_t) are the density of free and trapped electrons (holes) respectively. The densities of carriers injected into the i-layer, $N^{\pm}$, are large, so that as a first approximation one has:

$$N^{\pm} \cong \frac{CV}{eL}\frac{\tau_n}{t_n} = \frac{CV}{eL} G_d, \qquad (2.2)$$

where $G_d = \frac{\tau_n}{t_n}$ is the gain. Under a uniform photo-generation rate g_{ph}, if there are no interface effects, and when the electron mobility is larger than the hole mobility, the bulk controlled photogain, G_{ph} can be written as

$$G_{ph} \approx \tau_n/t_n \approx j_{ph}^F/j_{ph}^R \approx \mu_n\tau_n V/L^2 \qquad (2.3)$$

where the forward bias photocurrent $j_{ph}^F = e\, g_{ph}\, \mu_n\tau_n\, V/L$, and the reverse photocurrent $j_{ph}^R = eLg_{ph}$. The ratio j_{ph}^F/j_{ph}^R is the photogain, and is a direct measure of the electron mobility-lifetime product, $\mu_n\tau_n$. The reverse photocurrent should be measured with a high enough voltage so that all the generated photocarriers are collected.

The wavelength, λ, was varied to measure the spectral photogain $G_{ph}(\lambda)$. $G_{ph}(\lambda) = J_{ph}(\lambda)/eF(\lambda)$, where $J_{ph}(\lambda)$ is the measured photocurrent and $F(\lambda)$ the absorbed flux inside the device. The primary photocurrent space charge Q_{ph}, defined as $Q_{ph} = \int_0^L e(N_{ph}^+(x) - N_{ph}^-(x))dx$, where $N_{ph}^+(x)$

or $N^-_{ph}(x)$ are the primary photocarrier densities, moving and trapped, at x, is obtained from the photogenerated carrier gradient throughout the thickness of the device. If the primary photocurrent is assumed to be independent of the wavelength, then Q_{ph} becomes smaller when the absorption length decreases. As the bulk-induced secondary photocurrent is roughly proportional to Q_{ph}, then the bulk-induced photogain should decrease at short wavelengths when the absorption length decreases. In contrast, if the photogain is interface-induced, it will be flat or will go as $1/L_a$, where L_a is the absorption length (i.e. increase at short wavelength). The flatness or the variation as $1/L_a$ depends on the interface mechanism, but it never can vary as L_a in the case of an interface effect. Therefore, a flat photogain with L_a, or increase at short wavelength, is a clear indication of interface-induced photogain.

II.2 Experimental results

a-Si:H n-i-p and p-i-n devices were deposited at 200°C on SnO_2 coated glass substrates by rf glow discharge (13.56 MHz) in a hot-wall multiplasma monochamber reactor [19] , at Palaiseau. Structures grown on semitransparent Cr contacts thermally evaporated on glass substrates were also used to study a possible injection limitation at the substrate/n-type a-Si:H interface: no effect was found. The intrinsic layer thicknesses ranged from 1.0 to 3.0 microns, with a density of dangling bonds of $5x10^{15}$ cm^{-3}. Both the n- and p-layer were 200 Å thick. We have modified some n-i interfaces by interposing either a buffer layer of 20 Å thick SiN deposited at 250 °C, or a buffer of a slightly p-doped 300 Å layer. Cr or Al were used for the top contacts. A 300 Å semi-transparent Cr layer was used as the top contact for optical measurements.

Large photogain in an n-i-p structure

We have measured I-V curves of n-i-p and p-i-n diodes under forward bias with and without light-bias. We found that the photogain, G_{ph}, can be as high as 1000 in an n-i-p structure.

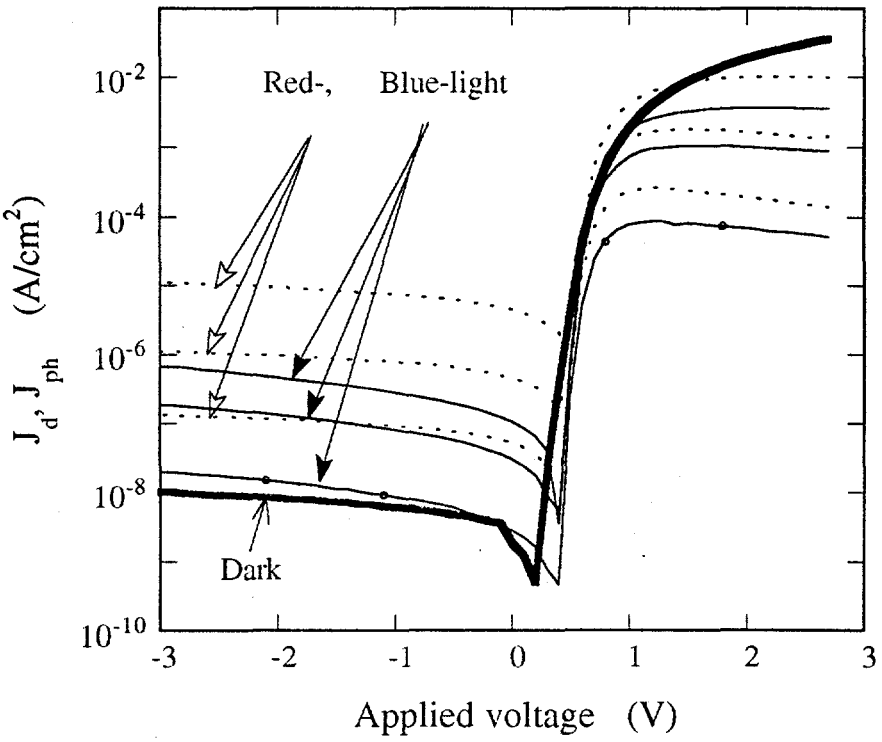

Fig. 8 Dark-current J_d and photo-current J_{ph} as a function of applied voltage for a 2 μm n-i-p diode illuminated on the n side, at various photon fluxes, for red (λ=650 nm) and blue (λ=450 nm) light

Figure 8 shows typical dark- and photo- J-V curves for a 2 μm n-i-p diode illuminated on the n side, at various photon fluxes, for red (λ=650 nm) and blue (λ=450 nm) light. The thick line is the dark current, the dotted lines are the photocurrent response for red light, and the thin lines are the photocurrent response for blue light. The saturation with V of the reverse bias photocurrents for red light indicates that we have a good measurement of the incident photon-flux, as required by Eq. (2.3). One can see that the forward-bias secondary photocurrents are much higher than the reverse-bias primary photocurrent. The photogain, according to Eq. (2.3), is about 1500 for red light but about 4500 for blue light in this sample. (the photogain should be small for blue light if it is a bulk effect.) The photogain decreases slightly at higher flux, when the forward-bias photocurrent becomes comparable to the dark current. One reason for the larger photogain under blue light is that the reverse photocurrent has not yet saturated at -3V. If the blue light intensity were corrected for the lack of saturation, the blue and red photogains would be roughly equal.

Interface-controlled photogain

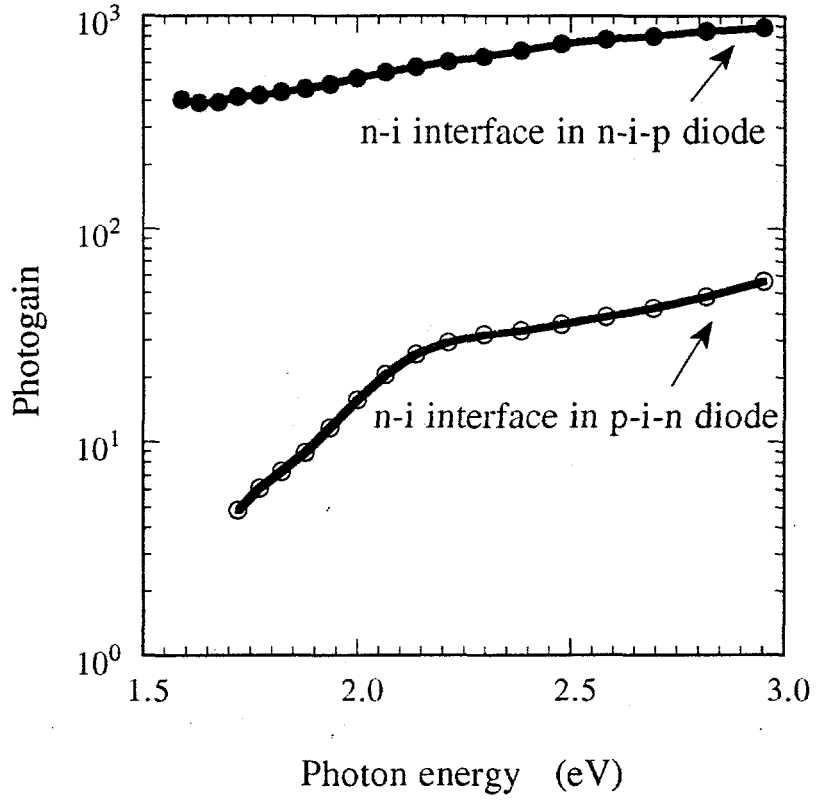

Fig. 9 Comparison of the photon-energy spectrum of the photogain for a 1.0 μm n-i-p and a 2.3 μm p-i-n diodes illuminated from n-i side

In contrast to the large photogain in n-i-p devices, we found there is only a very small photogain in p-i-n devices, produced either at Ecole Polytechnique or at other laboratories. In order to determine the origin of the photogain, we studied its photon energy dependence.

In Figure 9, we show the photon-energy spectra of the photogains for a 1 μm n-i-p device and a 2.3 μm p-i-n device (the latter was the only p-i-n sample to show photogain), both illuminated from the n-side. One can see in Fig. 9 for both the n-i-p and p-i-n devices , the photogains are somewhat flat as the photon energy varies from 3.0 eV to 2.0 eV. An even larger photogain for

blue light in an n-i-p device is shown in Figure 8. Surprisingly, among all the n-i-p devices we measured, we have never observed a photogain reduction under blue light, as expected for bulk-recombination-controlled photogain. It was always flat or increasing as the photon energy is increased. In Fig. 10, we compare the photogain spectra of the same p-i-n device as in Fig. 9, but illuminated from both the n-side and p-side. Here we have plotted the photogain as a function of the absorption depth. The photogain spectral response measured from both sides exhibits the same trend of high gain near the n-i interface but again low near the p-i interface. The results in Figs. 9 and 10 show first that the photogain in a p-i-n device is much lower than in an n-i-p device, and second that the photogain decreases from about 40 to less than unity as the absorption moves from near the n-i interface to near the p-i interface in this p-i-n device. This excludes a p-i interface photogain for these devices, as then exhibit no apparent bulk-induced photogain, and emphasizes the n-i interface effect. If a bulk-induced photogain exists in either an n-i-p device or a p-i-n device, it must be small: we have no indication for p-i-n device, we observe a dominant n-i interface effect on the photogain for n-i-p device, and the bulk photogain shoud be similar for n-i-p and p-i-n devices of the same thickness deposited under the same conditions.

Both the dark- and the photo-current responses of the devices strongly depend on the deposition sequence (n-layer before or after i-layer) which affects both n-i and p-i interfaces. One explanation of our findings is that the photogain in both n-i-p or p-i-n structures is controlled by the strength of the hole trapping near the n-i interface. This suggests that the n-i interface degrades by light-soaking as the bulk does. We also found that the recombination mechanism near the n-i interface is bimolecular for as-deposited devices, and becomes monomolecular after degradation.

The observation of photogain at short wavelengths when illuminated from the n side is a clear indication that the dominant contribution to the photogain is not from the bulk, but from the n-i interface. One possible explanation is that the n-i interface barrier is reduced by hole trapping. This can be understood as an enhanced electron injection due to the light-induced reduction of the n-i barrier. The photogenerated electrons in the junction depletion region are swept out by the strong internal electrical field, and the holes neutralize the negative junction space charge to lower the interface barrier. Moreover, the holes generated in the bulk by red light are collected at the n-i barrier and therefore contribute to the reduction of this barrier. It therefore appears that, at least in devices showing photogain, the electron injection is limited by the n-i barrier. The decrease of photogain at short wavelengths, for p-side illumination (see Fig. 10), is a clear indication that there is no photo-enhanced-injection at the p-i interface. As the p-i interface barrier is higher than the n-i interface barrier, and the electron trapping efficiency is not as high as the hole trapping efficiency, the negligible photo-effect at this interface is understandable. Moreover, as the dark electron current is much larger than the hole current, this dark current could inhibit a photo-effect at this interface. Further measurements of photon energy dependence of photogain on both p-i-n and n-i-p structures are needed to verify our hypothesis.

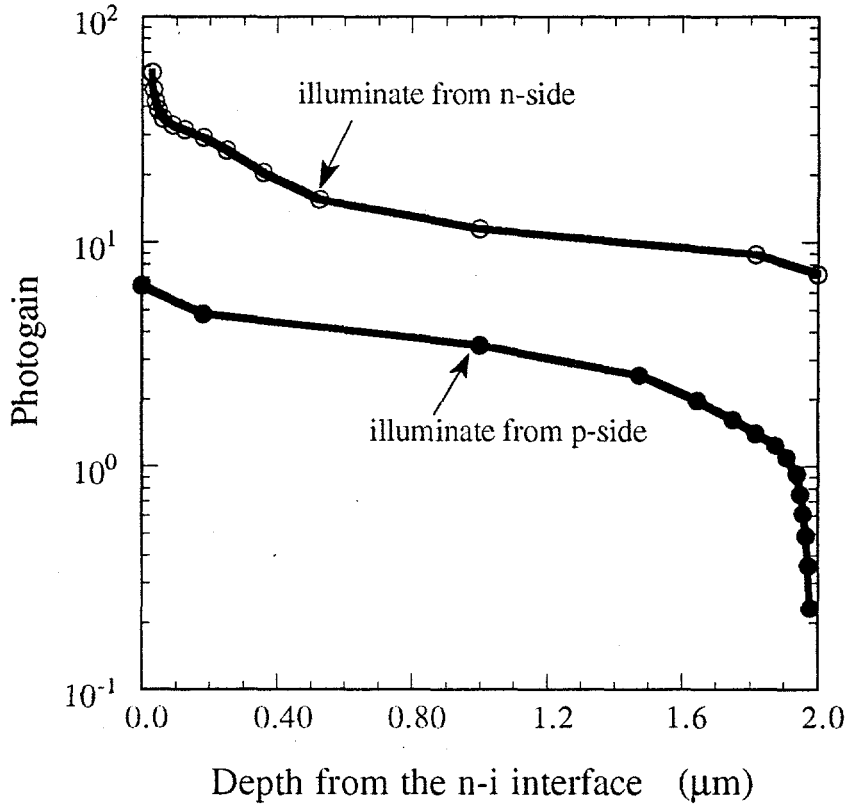

Fig. 10 Photogain as a function of absorption depth for a 2.3 μm p-i-n devices, which shows Gph is high near the n-i interface but low near the p-i interface, when illuminated from either the n-side or the p-side.

II.3 Conclusions

(1) We have observed a photogain, G_{ph}, as high as 1000 in a-Si:H n-i-p diodes for blue- and red- light generation. However, G_{ph} is below the limitation of our measurements in most of the p-i-n structures. This photogain in our n-i-p devices is attributed to the n-i interface, through a barrier-height reduction by trapped holes. The absence of photogain in the p-i-n devices may be attributed to p-i interface injection limitations.

(2) We have studied the photogain in 1- to 3-μm thick p-i-n and n-i-p samples, in which the photogain is unlikely to be related to the i-layer properties but is due to the interface effect. In the beginning of this work we attempted to study the transport parameter $\mu\tau$ product in the i-layer of a p-i-n structure; it is turned out that we observe instead the adjustment of the interface barrier by photocarriers.

III. Electronic Profiling

III.1 Null-current method

One of the consequences of the SWE is the change in the electric field distribution which affects the quantum efficiency wavelength dependence. It is important to determine how the electric field changes upon light-soaking. Basically, one applies a low intensity pulsed laser excitation of a specific wave length and consequently a specific absorption coefficient $\alpha(\lambda)$. Also applied is a voltage pulse in which the amplitude of the voltage in adjusted until there is no current due to the laser light. One then deduces the field profile by varying $\alpha(\lambda)$ and the applied voltage which gives a null current; e.g.

$$j_L = 0 = \int_0^L [E_i(x) - V_a/L] e^{-\alpha x} \, dx \qquad (3.1)$$

where V_a is the applied voltage which make $j_L = 0$ and $E_i(x)$ is the internal electric field profile.

M. Silver and his colleague[9] made electric field determinations in a Schottky-barrier cell by the null-current method using equipment at the Army Research Office. During the last contract year, we have set up a pulsed dye laser system on an optical table in our laboratory, and started to test the transient photocurrent signal from a-Si:H samples. The dye laser and optical table were supported by our department. We further showed that the null-current method works in p-i-n structures. However, the signal/noise ratio is low, and the measurement procedure is complicated because one has to change the dye many times for each curve. To do extensive measurements we need to buy, at least, a series of dyes and optical cells.

III.2 Carrier recombination studied by PL and EL spectroscopies in p-i-n diodes

We have collaborated with L. E. McNeil to study carrier recombination in a-Si:H p-i-n devices by using both PL and EL spectroscopies. A paper entitled "Carrier recombination in a-Si:H p-i-n devices studied by PL and EL spectroscopies" has been presented at the MRS spring meeting, in San Francisco in April 1995.

PL is the result of radiative recombination near the interface, while EL is a effect including both the bulk and the interfaces. The generation depth of electron-hole pairs can be varied by changing the wavelength of the laser beam in the PL measurements.

Both intensity and energy spectra of PL and EL were studied at temperature ranges of 80 to 300 K on a-Si:H p-i-n structures. We found [1,3,5] that the EL spectrum line shape depends on several parameters, such as the i-layer thickness, the generation rate, and the sample structure with or without a buffer layer (b-layer); while the PL spectrum line shape shows no difference those parameters are varied.

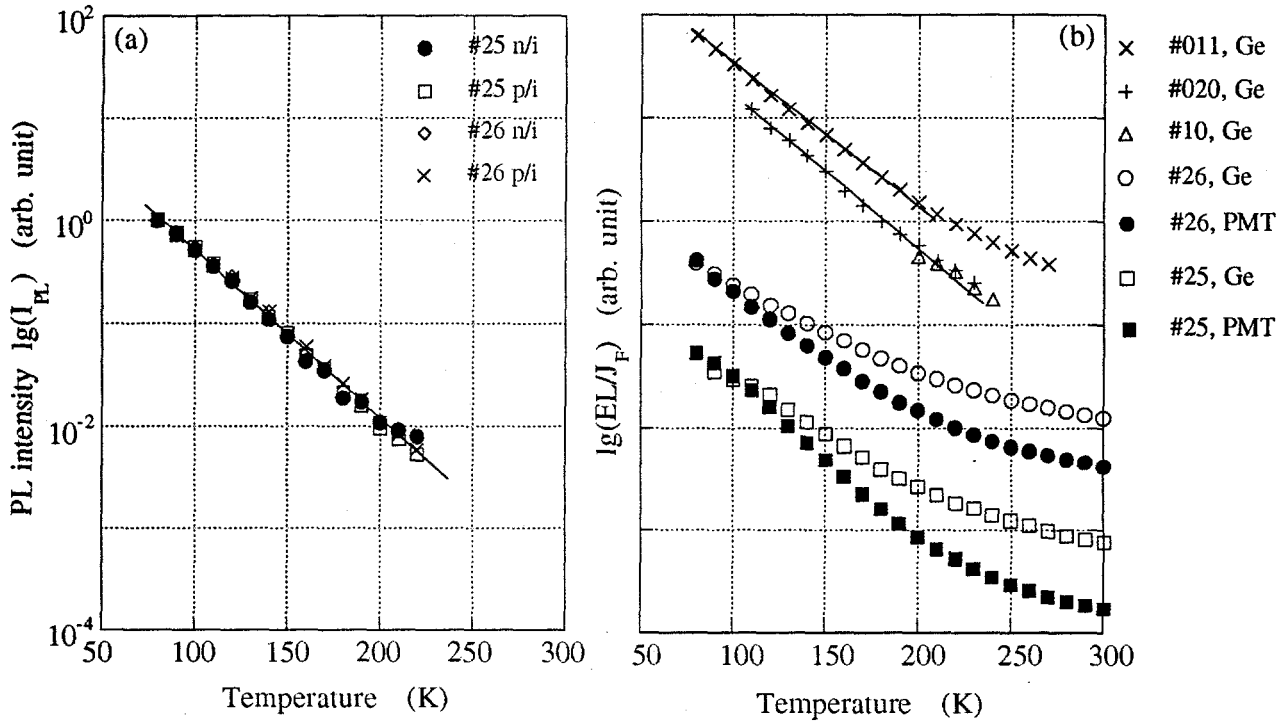

Fig. 11 Luminescence efficiency vs. T in 0.4 μm p-i-n and p-b-i-n samples #25 and #26
(a) PL from both n-i and p-i sides, and
(b) EL/J_F at 3 V applied voltage. EL/J_F data from 1.1, 2.0 and 10 μm p-i-n samples at 10 V, 12 V, and 30 V, respectively, are shown on the top.

Generally, the temperature dependence of the luminescence efficiency is a measure of the band-tail width in a-Si:H. It was found that the PL efficiency, $I_{PL}(T)$, decreases with increasing temperature in the range of 80 K < T < 300 K and follows the relation [10]

$$I_{PL}(T) = I_{PL0}\exp(-T/T_L) \qquad (3.2)$$

where $T_L = T_0/\ln(\nu_0\tau_r) \approx T_0/23$ with $\nu_0 = 10^{13}$ s^{-1} and an average radiative lifetime $\tau_r \approx 10^{-3}$ s. T_L is characterized by carriers which are trapped in the tail states, and T_0 is characterized temperature of the exponentially-distributed band tail states, $g(E) = g_0\exp(-\Delta E/kT_0)$. In intrinsic a-Si:H T_L is 20 - 25 K, corresponding to a T_0 of 460-575 K. In this model only tail-to-tail transitions were taken into account. This is the case in low-defect dendity a-Si:H films excited by band-gap light.The PL intensity as a function of temperature is shown in Fig. 11a for 0.4 μm p-i-n and p-b-i-n samples #25, and #26 excited from both the p-i and n-i sides. All the data fit to a straight line with a slope of $T_L \approx 26$ K. The results are consistent with previous PL studies in a-Si:H films.[6, 10] In comparison, EL/J_F as a function of temperature measured under constant voltage conditions is shown in Fig. 11b. The legend is listed on the right side of the figure. The top two curves are from thick samples. They give a slope of 27-29 K, close to the number from the a-Si:H films. However, the EL/J_F vs. T curves from thin samples #25 and #26 do not show a straight line. They are close to a straight line between 100 K < T < 200 K, with a much larger slope of 38 K and 48 K for samples #25 and #26, respectively. In order to exclude the defect-band luminescence the curves were measured by a 1.1 eV cut-off photomultiplier (PMT) instead a Ge detector, and these measurements are shown with solid circles and solid squares. A smaller slope of 30 K and 36 K for samples #25 and #26 was obtained. This indicates that defect luminescence does contribute, but the EL/J_F vs. T curves still show a weaker temperature dependence in thin p-i-n samples.

Why is the EL spectrum line shape sensitive to several parameters, such as the i-layer thickness, the generation rate, and the sample structure with or without a buffer layer, but PL is not? Why does the EL efficiency have a weaker temperature dependence than PL does? One reason is that the occupation of the tail states depends on how the carriers were excited, i.e., photon, electrical field, etc. The lower the energy of the luminescence main-peak, the less likely is the luminescence to grow with decreasing temperature.

III.3 Conclusions

(1) We have studied carrier recombination in a-Si:H p-i-n devices using both PL and EL spectroscopies, and found that the EL spectrum line shape depends on several parameters, such as the i-layer thickness, the generation rate, and the sample structure with or without a buffer layer (b-layer); while the PL spectrum line shape shows no difference those parameters are varied. The EL efficiency has a weaker temperature dependence than the PL does.

(2) PL from solar cell structures shows the same features as that in films, such as that the PL spectrum line shape does not change obviously with absorption depth or with either p/i or n/i interfaces, because the tail-to-tail transitions dominate the PL signal with band-gap light excitation.

IV. Transient Forward Current (TFC)

IV.1 Negative bias dependence of TFC

We have demonstrated extremely long relaxation times of the forward current decay of a-Si p-i-n devices [11,12]. In order to check whether the slow relaxation is due to the deep traps in the bulk or at the junctions, we have measured the TFC response after negative bias for p-i-n devices with different i-layer thickness of 0.4, 2.0 and 10 μm. We found that the thicker the i-layer, the larger the negative bias effect. So we conclude that this is a bulk effect. The negative-bias effect on the TFC in real solar cells, for which the i-layer thickness is about 0.4-0.5 μm, is not as obvious as that in thicker samples.

We have done more TFC measurements on p-i-n diodes made with or without H_2-dilution. They show very different features. To analyze the data and compare with the EL spectra results would result in more useful information about how different the deep traps are in these two types of cells.

IV.2 Applied voltage dependence of TFC in p-i-n and n-i-p solar cells

We have collaborated with G. J. Adriaessens at K. University Leuven, Belgium to study the transient forward current in several specimens of a-Si:H p-i-n structures as a function of bias voltage, temperature, and illumination as well as the degradation of the samples. We have continued to study the TFC in samples made at Solarex and ECD. The sample parameters are listed in Table I. The general features of TFC are a decaying initial electron-space-charge-limited current (SCLC) followed by a rise of recombination-limited current (RLC). We studied the TFC in several specimens of a-Si:H p-i-n structures as a function of bias voltage. Fig. 12 shows the forward-transient current from a high-efficiency solar cell #522.

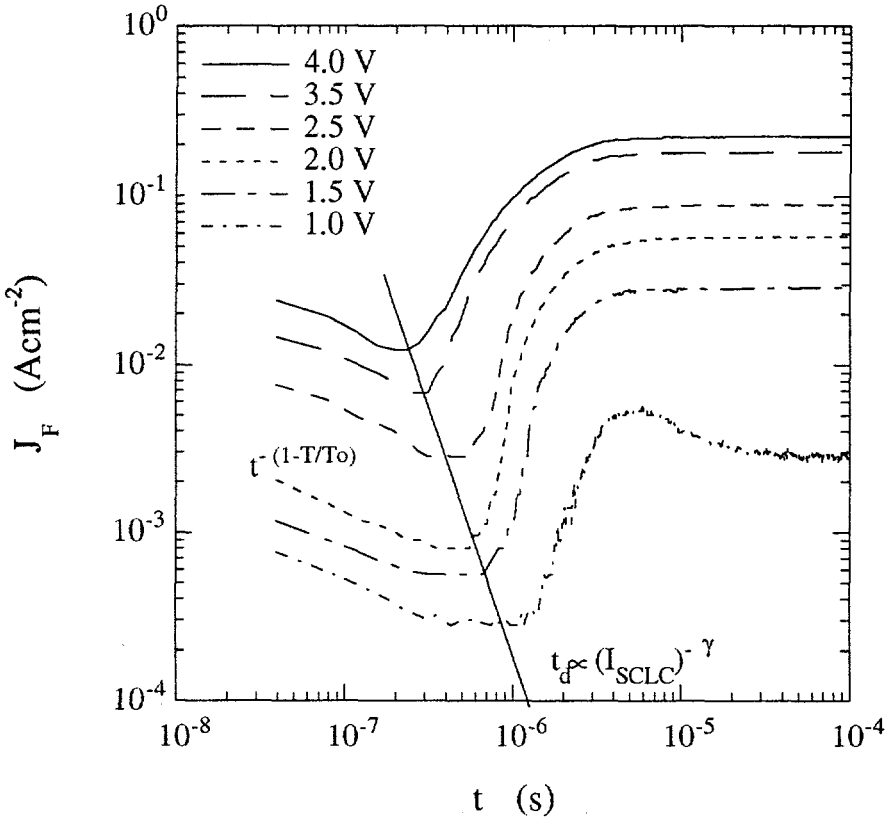

Fig. 12 Transient forward current as a function of applied voltage under 0.5 Hz pulses at 300 K for #522 cell

How much may we learn from these curves in Figs 12 and 13? The following information of gap states of the i-layer and interfaces can be obtained from TFC.

(A) As shown in Fig. 12, for a good injecting junction, the electron SCLC decays as a power law $I(t) \propto t^{-(1-\alpha)}$ where $\alpha = T/T_0$. T_0 is related to the density of gap states, so it is sensitive to light-soaking. It is consistent with our prevous results [13] that is the slope of the deep tail states below the conduction band edge changes with light-soaking. Since electron drift mobility $\mu_d(t)$ at longer times depends on the density of deeper states, the change of the slope in SCLC could be attributed to a change of T_0 according to $\mu_d(t) \propto (\nu_0 t)^{-(1-T/T_0)}$. T_0 = 340 and 750 °K, were found [13] for a 2 μm p-i-n at state A and B, respectively. For a poor injecting junction, the initial SCLC is either very low or shows a curved feature.

(B) The delay time of the current onset from its initial decay is related to the initial SCLC, with a power law, $t_d \propto (I_{SCLC})^{-\gamma}$, where γ is a constant, which is insensitive to the measurement conditions but depends on the properties of devices such as the density of states in the intrinsic layer. Therefore, we suppose the γ value is a measure of the quality of devices. For example, $\gamma \approx 0.7$ in the annealed state A but 1.7 in the light-soaked state B for a 3.7 μm p-i-n device.

(C) As seen in Fig. 12, the lowest curve under 1.0 V shows an overshoot of the recombination current onset at low field when the applied external electric field just balanced the built-in field. The overshoot becomes more pronounced in light-soaked states. The integral of the area, $\int \Delta J_F(t)dt$, is related to the density of deep states.

(D) As seen in Fig. 13, the value of the final recombination current multiplied by the rise time of the recombination current, J_{Ft_r}, is a constant, which indicates how much charge must be neutralized before the recombination current reaches a steady-state value. This number is small in high-efficiency cells but large in relatively-low-efficiency cells.

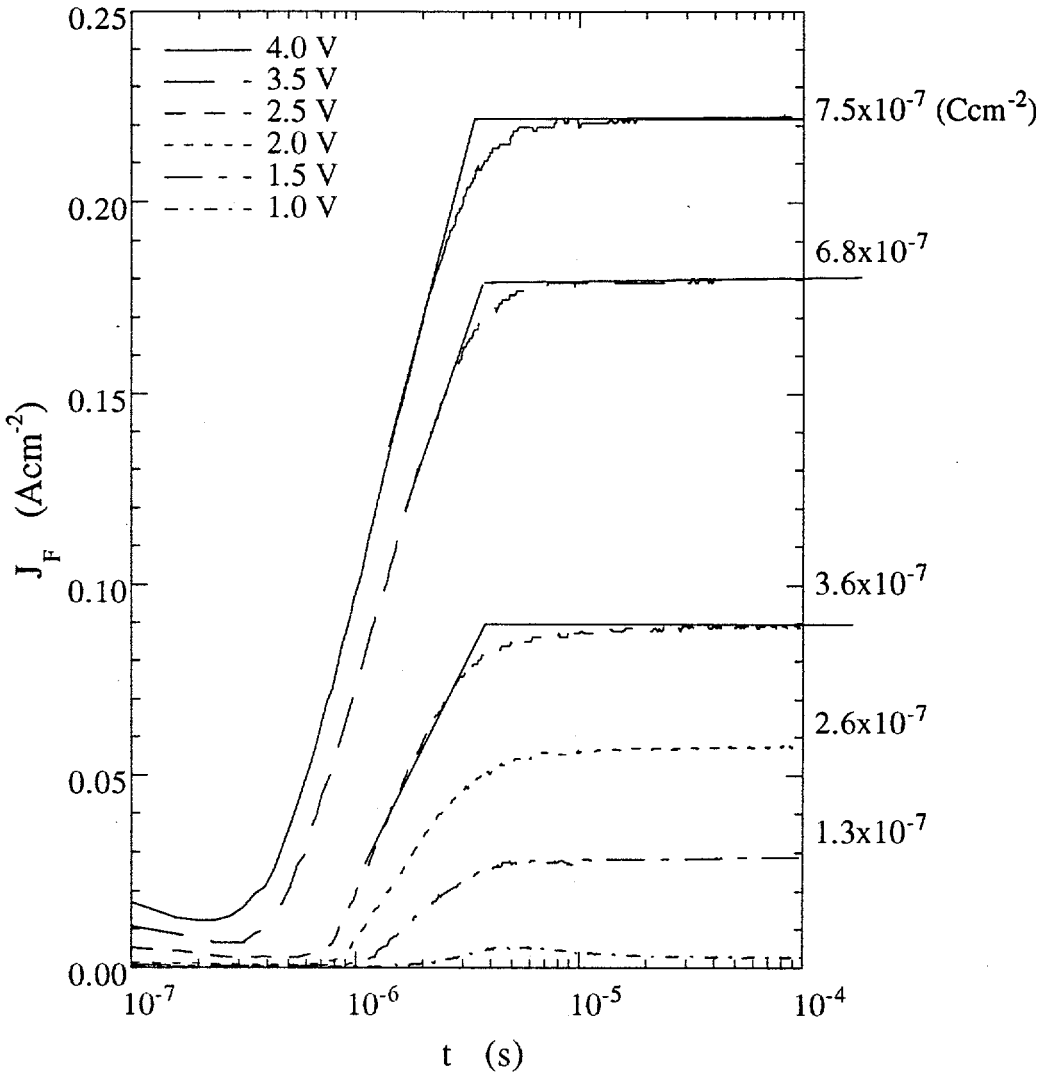

Fig. 13 The final forward current multiplied by the rise time of recombination current, , J_{Ft_r}, as a function of applied voltage, which shows a constant. The data are from the same sample as in Fig. 12

IV.3 Conclusions

1) For a good injecting junction, the electron SCLC decays as a power law $I(t) \propto t^{-(1-\alpha)}$ where $\alpha = T/T_0$. T_0 is related to density of gap states, so it is sensitive to light-soaking. According to the multiple-trapping model, [14] in a 0.4-0.5 μm sample under 1-2 V applied voltage, the demarcation energy sweeps the energy range of 0.23 to 0.35 eV below conduction edge in the time period of 10^{-8} - 10^{-6} sec at room temperature.

Considering that the conduction band tail has the form of a sum of two exponentails [15,16] the change of T_0 upon light-soaking can be explained by a change of the slope of the deeper exponential states.

2) The value of the final recombination current times the rise time of recombination current, $J_F t_r$, is close to a constant which is in the order of 10^{-7} Ccm^{-2} in high efficiency cells but is greater than 10^{-6} Ccm^{-2} in relatively low efficiency cells.

V. Modeling

We presented a simple model to explain our TFC data in section IV["Forward current transients in amorphous silicon p-i-n structures", to be published in J. Non-Cryst. Sol.(1995)]. We studied the EL intensity as a function of forward current in a group of p-i-n devices in a wide temperature range. We found that the linearity occurs only under certain conditions. In most cases, there is either sublinear or supralinear dependence of EL on current. [see publication 1]. We observed a distinct recombination regime in amorphous silicon diodes under double injection [see publication 2].

We discuss the appropriate generation rate for analysis of EL in this section. Generally, the steady state EL intensity, I_{EL}, is defined as the number of photons per unit volume per second produced from the sample. Since the energy of the emitted photons is less than 1.6 eV, the internal re-absorption is negligible for a sample thickness less than 10 μm. The EL quantum efficiency, $\eta = I_{EL}/g$, is defined as the ratio of EL intensity, I_{EL}, to the generation rate, g. It is common to calculate an effective generation rate g for an EL from the forward bias current density. Then, $g = J_F/eL$ where J_F is the forward-bias current density, e is the charge of an electron, and L is the i-layer thickness. This is valid if every carrier across the junction recombines within the device. In other words, if the carrier recombination lifetime τ is less than or equal to the transit time t_0. When the condition $\tau \le t_0$ is not met, this expression $g = J_F/eL$ is questionable. When the injection current is larger than the recombination current, gain $(\tau/t_0) > 1$, the forward bias current is approximated by

$$J_F = \frac{CV}{t_0}\frac{\tau}{t_0} = J_r\frac{\tau}{t_0}, \qquad [\text{A cm}^{-2}] \qquad (5.1)$$

where C is the sample capacitance, V is the voltage across the i-layer. This implies that before one injected electron recombines with a hole in the device it circulates in the circuit τ/t_0 times. In the dark, we obtain the gain factor $(\tau/t_0) = (\mu\tau E)/L$ where E is the electrical field across the i-layer, and $t_0 = L/(\mu E)$. So the generation rate for EL can be expressed as

$$g = \frac{J_F}{e\mu\tau E}. \qquad [\text{cm}^{-3}\text{s}^{-1}] \qquad (5.2)$$

Then one should use for the EL efficiency

$$\eta = \frac{I_{EL}}{J_F/eL}\left(\frac{\tau}{t_0}\right). \qquad (5.3)$$

In Eq. (5.2) and (5.3) the drift-length $\mu\tau E$ is substituted for the sample thickness L in the commonly used expression $g=J_F/eL$.

This same argument can be made in another way. Because the electron-current contribution dominates the total current in a-Si:H p-i-n diodes under double injection, the forward current can be written as

$$J_F \cong J_n = en\mu_n E \qquad [A\ cm^{-2}]$$

$$= eg\mu_n\tau_n E, \qquad [A\ cm^{-2}] \qquad (5.4)$$

where $\mu_n\tau_n$ is the mobility-lifetime product for electrons. So the effective generation rate for EL can be written as

$$g \cong \frac{J_F}{e\mu_n\tau_n E} = \frac{J_F}{eL_D} \qquad [cm^{-3}s^{-1}] \qquad (5.5)$$

The EL quantum efficiency I_{EL}/g can be expressed as

$$\eta \cong \frac{I_{EL}}{J_F/eL_D} \qquad (5.6)$$

where $L_D = \mu_n\tau_n E$ is the electron drift-length. In Eq. (5) and (6) the electron drift length prior to recombination, $\mu_n\tau_n E$, is used instead of $\mu\tau E$ in Eq. (2) and (3). The drift-length, $\mu\tau E$, must be much greater than the i-layer thickness in a good solar cell, therefore, the gain factor, $(\tau/t_0) = (\mu\tau E)/L$, must be much larger than unit and the actual generation rate of EL should be much smaller than the commonly used number, J_F/eL. The measured EL efficiency, therefore, is comparable to that of PL.

The importance of suitable definitions for the generation rate has been seen in Section I Figs 6 and 7. However, both the J_F - V characteristics and $\mu\tau$ shall change with photodegradation, and they change with temperature as well.

VI. New material studied by Nuclear Magnetic Resonance (NMR)

VI. 1 Experimental results

We have observed preliminary NMR results for the structure of hot-wire material that has shown improved stability. Hot-wire film TH125 was deposited on Al foil at NREL. The film was peeled off by DI water diluted-HCl. A proton-free probe was used for the NMR measurements. Fig. 14 shows the NMR spectrum in a hot-wire sample. A two-component lineshape is ubiquitous, as observed for all a-Si:H films. The narrow component is associated with randomly distributed monohydride groups, the broad component is associated with the clustered monohydride groups. Other local hydrogen bonding configurations also contribute to the broad component. The NMR lineshape in a conventional PECVD a-Si:H sample contains about 70% broad component. However, in the hot-wire sample, the percentage of the broad band was lower than 50% of the total resonance signal. This means these must be much less clustered -H, dihydrides, trihydrides, and polymeric $(Si\text{-}H_2)_n$ in the hot-wire film. This is experimental evidence that the hydrogen local bonding configuration plays an important role in photodegradation effects. The randomly-distributed monohydride group is more stable than other hydrogenated bonding configurations.

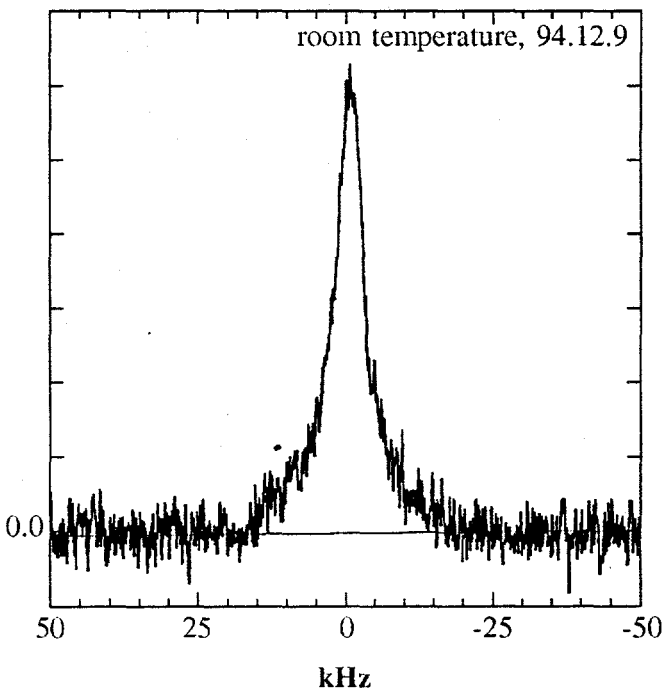

Fig. 14 the NMR spectrum in a hot-wire sample.

VI. 2 Conclusion

The NMR lineshape in a conventional PECVD a-Si:H sample contains about 70% broad component. However, in the hot-wire sample, the percentage of the broad band was lower than 50% of the total resonance signal. This means there is much less clustered-H in the hot-wire film. This is experimental evidence that the randomly distributed monohydride group is more stable than other hydrogenated bonding configurations.

CONCLUSIONS

I. Summary of the answers for the questions arising in the beginning of the introduction

1. Are the important states related to the SWE located primarily near the junctions or are they located in the bulk of the i-layer?

This is an important issue for a-Si:H PV industry. Our answer is that the important states related to the SWE are located primarily in the bulk of the i-layer. We have shown evidence from EL spectrum studies of p-i-n solar cells. There is no doubt that under double-injection conditions the measured photons are emitted from the 0.4-0.5 μm i-layer. We have measured the light-soaking effect on EL spectra in several groups of solar cells, and have shown the decrease of main-band and the increase of the defect-band luminescence (Chapter I). The results can be explained by an increase of deep states in the i-layer. Depending on the charge state of these deep states, they act as either non-radiative or radiative recombination centers. The increase of the non-radiative centers quenches the main-band luminescence, while the increase of the radiative centers enhances the defect-band luminescence.

Furthermore, we cannot exclude the light-induced effects near the junctions. Most of the states near the junctions are deep states. They may directly or indirectly contribute to SWE. Since we konw that the EL effective efficiency at room temperature is proportional to the solar cell initial efficiency. And the EL efficiency is inversely proportional to the defect density in both the i-layer and the interfaces, the interface contribution can be evaluated with the known bulk density of defects.

2. How do the metastable changes of deep states correlate to the photodegradation of the solar cells?

From section 1.3 we have learned that the EL spectra of the photodegradation effect give useful information about how those deep states are responsible for the degradation. In cooperation with Solarex we are attempting to further characterize the nature of such defects using EL spectroscopy to measure the energy distribution of defects and their photodegradation kinetics in a-Si:H solar cells made with and without H_2-dilution.

It has been found that the photoinduced degradation of solar cells with two types of defects, "fast" and "slow", which are present in a-Si:H made with pure silane. In contrast, a-Si:H made with H_2-dilution appears to have predominantly the "fast" states only.[17,18] EL spectra of the photodegradation effect in both H_2-diluted and non H_2-diluted solar cells is being undertaken in the same group of solar cells made at Solarex.

3. Whether or not the SWE related with non-relaxed states?

It is the case that the SWE occurs under non-equilibrium conditions. However, the arguments still continue.[19] One question is whether the defect relaxation takes place or not in a-Si:H,[19] the other is what is the origin of the SWE. [20] We have shown the defect relaxation did occur by optical-bias experiments. [21] We are attempting to work out a model of SWE with the relaxation phenomena.

II. Further effort

Efforts will be continued to cooperate with team members, especially members from the PV industry to study the factors governing the SWE in a-Si:H solar cells. We will pay more attention to the EL measurements, which give more directly useful information to this subject, and to the NMR measurements, which give structural information on the new hot-wire material.

Publications:

1. Keda Wang, Daxing Han, and M. Silver, "The Power Law Dependence of EL Intensity on Forward Current in a-Si:H p-i-n Devices", in Amorphous Silicon Technology, edited by E. A. Schiff, M.Hack, A. Madan, M. Powell, A. Matsuda, MRS Symp. Proc. **336** 861 (1994).
2. Daxing Han and Keda Wang, "A distinct recombination regime in amorphous silicon diodes under double injection", Appl. Phys. Lett. **66** (1995) 879.
3. Daxing Han and Keda Wang, "Electroluminescence from hydrogenated amorphous silicon p-i-n diodes" to be published in J. Non-Cryst. Sol.(1995).
4. Regis Vanderhaghen and Daxing Han, "Interface effects on double injection current and photocurrent in a-Si:H n-i-p and p-i-n diodes", to be published in J. Non-Cryst. Sol.(1995).
5. B. Yan, G.J. Adrianenssens, A. Eliat, and D. Han, "Forward current transients in amorphous silicon p-i-n structures", to be published in J. Non-Cryst. Sol.(1995).
6. Keda Wang and Daxing Han, in Amorphous Silicon Technology, edited by E. A. Schiff, M.Hack, A. Madan, M. Powell, A. Matsuda, MRS Symp. Proc. (1995).
7. C. N. Yeh, D. X. Han, K. D. Wang, and L. E. McNeil, in Amorphous Silicon Technology, edited by E. A. Schiff, M.Hack, A. Madan, M. Powell, A. Matsuda, MRS Symp. Proc. (1995).

References

1. "Recombination and Metastability in Amorphous Silicon and Silicon-Germanium Alloys", July 1994·NREL/TP-451-6491.
2. Research on Stable, High-Efficiency Amorphous Silicon Multijunction Modules, NREL/TP-411-7190, October 1994, p.34.
3. Keda Wang, Daxing Han, and M. Silver, "Thickness Dependence of Electroluminescence in a-Si:H p-i-n Devices", "Amorphous Silicon Technology", MRS proc.**297** 857-862 (1993).
4. Keda Wang, Daxing Han , M. Kemp, and M. Silver, "Time-resolved Transient Electroluminescence in a-Si:H," Appl. Phys. Lett.**62**, 157-159 (1993).
5. Daxing Han and Keda Wang, "Electroluminescence from hydrogenated amorphous silicon p-i-n diodes" to be published in J. Non-Cryst. Sol.(1995).
6. R. A. Street, in "Semiconductors and Semimetals", Vol 21B, edited by J.I. Pankove, Academic Press, Inc, 1984) p.199.
7. A. Rose, 'Concepts in Photoconductivity and Allied Problems', (Krieger, Huntington, New York, 1978). chapters 3,7.
8. R. R. Arya, A. Catalano, and R. S. Oswald, Appl. Phys. Letts. **49**, 1089 (1986).
9. T. Datta and M. Silver, Appl. Phys. Lett. 38, 903 (1981).
10. R. W. Collins, M. R. Paesler, and W. Paul, Solid State Commun. **34**, 833 (1980); R. W. Collins and W. Paul, Phys. Rev. **B25**, 5257 (1982).
11. Daxing Han, Keda Wang, and M. Silver, "Reverse Recovery and Decay of Stored Excess Carriers in a-Si:H p-i-n Diode," "Amorphous Silicon Technology", MRS Proc. **258**, 837-841 (1992)
12. Daxing Han, Keda Wang, and M. Silver, "Transient Forward Bias Current in a-Si:H p-i-n Devices", **164-166** 339-342 (1993).
13. Daxing. Han, Keda. Wang, and M. Silver, "Light Induced Metastable Defects in a-Si:H Studied by Transient Space Charge Perturbed Currents," J. Non-Cryst. Sol. **137/138**, 267-270 (1991).
14. T. Tiedje, in "Semiconductor and Semimetals", **21C**, edited by J. I. Pankove, (Academic Press. Inc. 1984), p.207-238.
15. C. Y. Huang, S. Guha, and S. J. Hudgens, Phys. Rev. **B27**, 7460 (1983).
16. M. Hack, S. Guha, and Shur, Phys. Rev. **B30**, 6991 (1984).
17. L. Yang and L. Chen, Appl. Phys. Lett. **63** (1993) 400.
18. L. Yang and L. Chen in "Amorphous Silicon Technology," edited by E. A. Schiff, M.Hack, A. Madan, M. Powell, A. Matsuda, (MRS Symp. Proc. **336** 1994) pp. 669-674.
19. W. B. Jackson and N. M. Johnson, in "Amorphous Silicon Technology," (MRS Symp.1995).
20. P. Tzanetakis, N. Kopidakis, M. Androulidaki, C. Kalpouzos, P. Stradins and H. Fritzsche, in "Amorphous Silicon Technology," (MRS Symp.1995).
21. Daxing Han, Douglas C. Mecher, E. Schiff, and M. Silver, "Optical Bias Effect on Electron-drift measurements and Defect Relaxation in a-Si:H," Phys. Rev. **B48**, 8658-8666 (1993).

REPORT DOCUMENTATION PAGE

Form Approved
OMB NO. 0704-0188

1. AGENCY USE ONLY (Leave blank)	2. REPORT DATE	3. REPORT TYPE AND DATES COVERED
	July 1995	Annual Subcontract Report

4. TITLE AND SUBTITLE

Experimental Study of the Factors Governing the Staebler-Wronski Photodegradation Effect in a-Si:H Solar Cells

5. FUNDING NUMBERS

C: XAN-4-13318-09

TA: PV531101

6. AUTHOR(S)

D.X. Han, L.E. McNeil, K.D. Wang, C.N. Yeh

7. PERFORMING ORGANIZATION NAME(S) AND ADDRESS(ES)

University of North Carolina
Chapel Hill, North Carolina

8. PERFORMING ORGANIZATION REPORT NUMBER

9. SPONSORING/MONITORING AGENCY NAME(S) AND ADDRESS(ES)

National Renewable Energy Laboratory
1617 Cole Blvd.
Golden, CO 80401-3393

10. SPONSORING/MONITORING AGENCY REPORT NUMBER

TP-411-8116

DE95009272

11. SUPPLEMENTARY NOTES

NREL Technical Monitor: W. Luft

12a. DISTRIBUTION/AVAILABILITY STATEMENT

12b. DISTRIBUTION CODE

UC-1262

13. ABSTRACT *(Maximum 200 words)*

This report describes continuing experiments on electroluminescence (EL) and transient forward bias current (TFC) as well as photocurrent before and after light soaking for amorphous silicon (a-Si:H) devices. We continued our EL spectrum analysis on a p-i-n device with and without SiC:H buffer in the p-i interface. We started a program to study the Staebler-Wronski effect (SWE) in p-i-n solar cells made with and without H_2 dilution, in collaboration with Solarex. In collaboration with L.E. McNeil, we studied the carrier recombination in p-i-n cells by both photoluminescence and EL. In collaboration with G.J. Adriaessens at Catholic University Leuven, Belgium, we studied TFC in p-i-n devices. In collaboration with Y. Wu, we studied the local Si-H bonding configuration in hot-wire samples by nuclear magnetic resonance. We concentrated on determining the factors controlling SWE, and on determining the correlation of EL data to the cell structure or preparation conditions, such as the effects of buffering and H_2 dilution, by EL measurements.

14. SUBJECT TERMS

Staebler-Wronski ; photodegradation ; hydrogenated amorphous silicon ; photovoltaics ; solar cells

15. NUMBER OF PAGES

31

16. PRICE CODE

17. SECURITY CLASSIFICATION OF REPORT	18. SECURITY CLASSIFICATION OF THIS PAGE	19. SECURITY CLASSIFICATION OF ABSTRACT	20. LIMITATION OF ABSTRACT
Unclassified	Unclassified	Unclassified	UL